The Effect of Interlayer Adhesion on the Mechanical Behaviors of Macroscopic Graphene Oxide Papers

Yun Gao,[†,‡] Lu-Qi Liu,[†,*] Sheng-Zhen Zu,[†] Ke Peng,[†] Ding Zhou,[†] Bao-Hang Han,[†,*] and Zhong Zhang[†,§,*]

[†]National Center for Nanoscience and Technology, China, Beijing 100190, P.R. China, [‡]Academy for Advanced Interdisciplinary Studies, Peking University, Beijing 100871, P.R. China, and [§]Center for Nano and Micro Mechanics, Tsinghua University, Beijing 100084, P.R. China

ABSTRACT High mechanical performances of macroscopic graphene oxide (GO) papers are attracting great interest owing to their merits of lightweight and multiple functionalities. However, the loading role of individual nanosheets and its effect on the mechanical properties of the macroscopic GO papers are not yet well understood. Herein, we effectively tailored the interlayer adhesions of the GO papers by introducing small molecules, that is, glutaraldehyde (GA) and water molecules, into the gallery regions. With the help of *in situ* Raman spectroscopy, we compared the varied load-reinforcing roles of nanosheets, and further predicted the Young's moduli of the GO papers. Systematic mechanical tests have proven that the enhancement of the tensile modulus and strength of the GA-treated GO paper arose from the improved load-bearing capability of the nanosheets. On the basis of Raman and macroscopic mechanical tests, the influences of interlayer adhesions on the fracture mechanisms of the strained GO papers were inferred.

KEYWORDS: graphene oxide · mechanical properties · Raman spectroscopy · interlayer adhesion · strain transfer

Owing to their remarkable thermal, mechanical, electrical, and optical properties, individual graphene nanosheets have been envisioned as novel nanoscale building blocks to create macroscale graphene-based architectures applied in energy storage technology,[1] composites,[2] mechanical actuators,[3] and optoelectronic devices.[4,5] Over the past few years, several approaches have been developed to produce individual graphene nanosheets including micromechanical exfoliation of graphite,[6] epitaxial growth through chemical vapor deposition,[7] bottom-up organic synthesis,[8] and chemical modification of graphite.[9] The major advantage of the first three methodologies is the high crystal quality of individual graphene sheets yielded, whereas the mass production of graphene remains a big challenge. Given that natural graphite is ubiquitous and inexpensive in large quantities, the chemical exfoliation of graphite turns out to be a facile and versatile option for the production of individual graphene sheets in large scale.[10] In addition, the solution-phase feature of chemically exfoliated graphene would also favor subsequent processability and wide-scale applicability.[11]

Graphene oxide (GO), as a well-known chemically exfoliated derivative, could be easily dispersed into a variety of solvents because of the presence of carboxylic and hydroxyl groups.[12] The planar feature of a GO sheet makes it easy to assemble into paper-like materials through simple filtration or liquid/air interface self-assembly.[13,14] Mechanical tests have indicated that GO papers exhibit superior stiffness and strength, which surpass most of carbon-based paper-like materials such as buckypaper and flexible graphite foil.[10] After further thermal annealing, the resulting paper displays a remarkable mechanical improvement together with high electrical and thermal conductivities.[15] It has to be pointed out that the mechanical properties of macroscale GO papers are still orders of magnitude lower than those of individual graphene sheets. Additionally, the reported both Young's modulus and ultimate tensile strength of GO papers, respectively, lay in a relatively wide range of 6−42 GPa and 76−293 MPa.[13−16] Such variance not only arises from the "size-dependent effect" of testing specimens, but also comes from the variety of stacked sheets construction manner and interactions in GO papers. It is still a big challenge in the material community so far as to how to create such hierarchically structured nanocomposite in which each sublayer contributes a distinct function to yield a mechanically integrated macroscopic material.

Recently, Ruoff and co-workers[17,18] have pointed out that chemically cross-linking between adjacent GO sheets would impose

* Address correspondence to zhong.zhang@nanoctr.cn, hanbh@nanoctr.cn, liulq@nanoctr.cn.

Received for review December 6, 2010 and accepted February 4, 2011.

Published online February 22, 2011
10.1021/nn103331x

positive or sometimes negative influence on the mechanical properties of GO papers. For example, the edge-bound divalent metal ions (*e.g.*, Ca^{2+}, Mg^{2+}) would result in the improved stiffness and strength of the papers, whereas the intercalated metal ions between the GO sheets would lead to a reduced mechanical performance owing to the increased layer-to-layer distance (*d*-spacing). In fact, the macroscopic mechanical properties of GO paper materials reflect the collective behavior of various factors, and thereby it is not correct to attribute the macroscopic mechanical variations to one individual factor. Furthermore, the dependence of mechanical properties of GO papers on water content,[19] interlayer interactions,[14] the wrinkle and waviness of sheets, and the packed degree of individual sheets cannot be studied only by conventional mechanical tests. Thus, we need develop a generic methodology independent of macroscopic mechanical measurements to help us explore the microscale structure's influence on mechanical properties of macroscopic GO papers.

On the basis of our recent works,[20,21] in which the *in situ* Raman microscope was successfully employed on monitoring the load-bearing capability of various carbon nanotube (CNT)-based macroarchitectures (*e.g.*, CNT film and fiber) at microscale level, the Young's modulus of CNT architectures was predicted and agreed well with the macroscopic mechanical performance. Analogous to the CNT samples, the strained graphene exhibited a linear relationship between the shift of specific Raman peaks and local strain.[22,23] In this work, we utilize the *in situ* Raman spectroscopy to investigate the influence of interlayer adhesions on the loading role of strained GO sheets for chemically derived GO papers. Small molecular adhesives, such as glutaraldehyde (GA) and water molecules, were introduced into the gallery regions between adjacent GO sheets which are expected to tailor the interlayer adhesions. By analyzing the variations of the Raman G band under strain, we can infer the structural fracture mechanisms of the GO papers, and further predict the moduli of the macroscopic papers. Furthermore, with systematic static and dynamic mechanical tests, we could elucidate the influence of their macroscopic mechanical performances on interlayer adhesions.

RESULTS AND DISCUSSION

GO nanosheets are synthesized from natural graphite powder *via* chemical exfoliation.[24] The atomic force microscopy (AFM) image of the GO suspension shown in Figure 1a offers a straightforward evidence for peeled-off single GO sheets. The thickness of nanosheets we prepared is within a narrow range of 1.1−1.2 nm, as indicated in the contour curve. Further Fourier-transformed infrared (FTIR) spectroscopy characterization demonstrated that the carboxylic, hydroxyl, and epoxide groups were successfully grafted onto the nanosheet

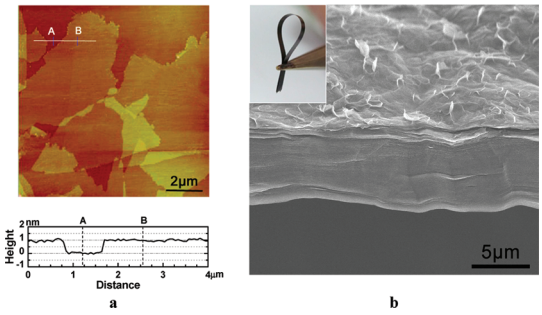

Figure 1. (a) AFM ichnography and cross-section contour of GO sheets; (b) SEM side-view image of the GO paper displays its well-packed structure, the inset is the digital picture of strip specimen for tensile test.

surfaces (Figure 2c). With the monolayered nanosheets as basic building blocks, the macroscopic GO papers were fabricated by the flow-directed filtration method. The cross section observations of a sample strip *via* scanning electron microscopy (SEM) in Figure 1b revealed the well-packed layer-structure of GO papers.

The existences of hydroxyl as well as carboxylic moieties on the surfaces of nanosheets (Figure 2a) make it possible to further chemically derivate the GO samples.[17,18] Herein, we employed GA molecules to covalently bond the neighboring GO nanosheets to strengthen the interlayer adhesion. The hydroxyl groups on the surface of nanosheets readily reacted with aldehyde groups of GA molecules through intermolecular acetalization.[25] The X-ray diffraction (XRD) patterns shown in Figure 2b indicate the intercalation of GA molecules into the gallery spaces, in which the *d*-spacing visibly increases to ~1.12 nm from the initial ~0.78 nm of as-received GO papers. FTIR spectra in Figure 2c are used to characterize the chemical modification of as-received GO papers. The peaks around 2800−3000 cm^{-1} correspond to the C−H stretch modes of the intercalated GA molecules. The intensity of C−O stretch mode at around 1100 cm^{-1} increases after the acetalization, implying the covalent linkage of GA molecules between the adjacent GO nanosheets. Furthermore, X-ray photoelectron spectroscopy (XPS) is utilized to elucidate the surface state of the GO paper before and after GA treatment as shown in Figure 2d. The C1s peak of the as-received GO paper can be fitted into five line shapes with binding energy at 284.8, 286.0, 287.0, 288.2, and 289.4 eV, corresponding to the C in graphite, C−OH, C(epoxide), C═O, and O−C═O groups. For the GA-treated GO paper, a new component (acetal groups) at 286.5 eV appears, together with the decrease of the C−OH percentage at 286.0 eV. These results again confirm that the GA molecules are covalently attached onto the GO surface and lead to enhancement of interlayer adhesion between the adjacent GO nanosheets. In addition, interlamellar water molecules have been reported to affect the mechanical properties of GO paper due to the modifying hydrogen networks.[19] Herein, water molecules were also utilized to tailor the interlayer adhesions of the GO papers. As

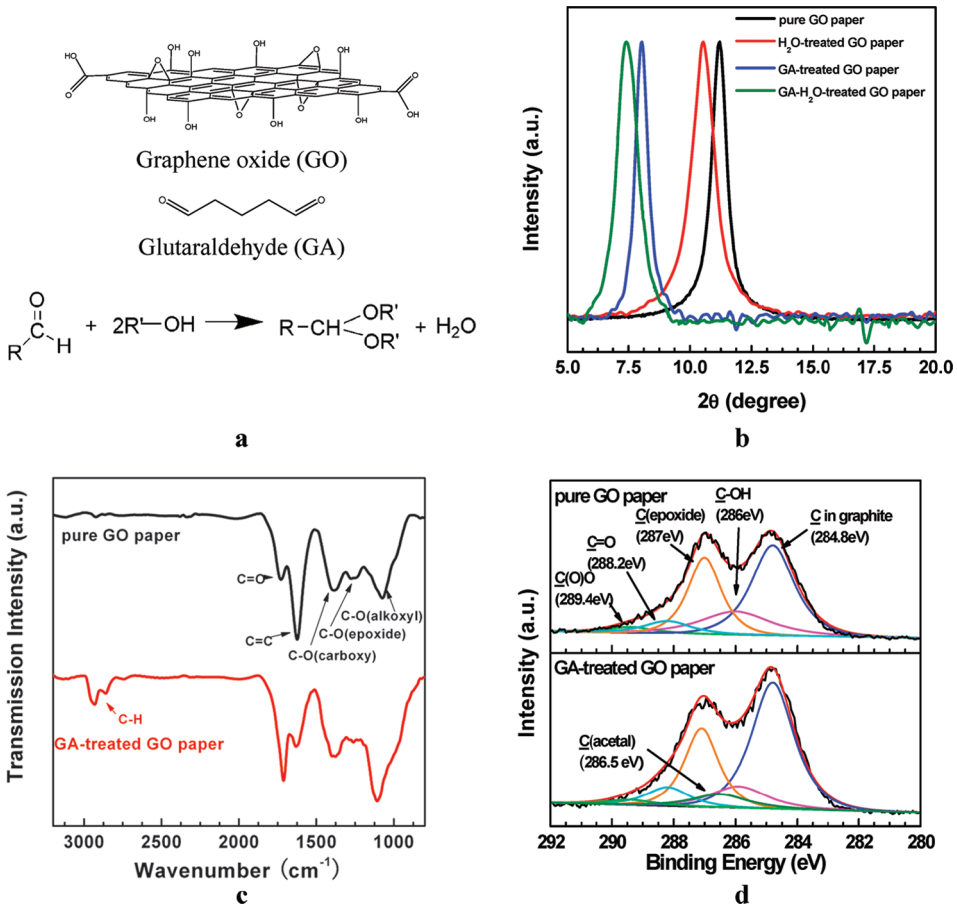

Figure 2. (a) Schematic model of GO sheet showing possible oxygen-containing functionalities, chemical structure of GA molecule, and schematic of acetalization of hydroxyl groups with aldehyde groups; (b) XRD patterns of GO paper samples that have been treated with various methods; (c) comparison of FTIR spectrum for the GO paper and GA-treated GO paper; (d) deconvoluted C1s orbital XPS spectra for the GO paper and GA-treated GO paper.

shown in the XRD patterns in Figure 2b, the slightly increased *d*-spacing for both the as-received GO paper and GA-treated GO paper after water adsorption at a relative humidity of 98% and 30 °C for 3 days illustrates the intercalation of water into the gallery spaces.

To unveil the load-bearing status of the GO nanosheets, we applied *in situ* Raman measurements on the strained macroscopic papers. Figure 3a shows the typical G band Raman spectra of the GO nanosheets, which obviously broaden as compared to the graphene sheets.[26,27] This asymmetrical broadening of the line shape could be ascribed to two reasons: (i) the D′ band (~1620 cm^{-1}), derived from defects, may partially merge with the G band; (ii) the symmetry breaking of the conjugated π systems of the GO samples arose from the introduced various functional groups, and then the G band itself would split. Herein, on the basis of the above analysis, the G band of GO paper was fitted well with three peaks of G^-, G^+, and D′. As the uniaxial tensile strains are applied onto the GO paper, the downshifts of the G band are expected, which arise from the weakening of the carbon−carbon bonds as a result of the elongated interatomic distance. Figure 3 panels b and c summarize the varied trends of the G^- and G^+ peak positions as a function of the applied strains for the as-received and GA-treated GO papers. Apparently, the downshift trends of the G^+ band are much less than that of the G^- band for both the GO paper and GA-modified paper. As discussed by Mohiuddin *et al.*,[23] the different shift trends of G^- and G^+ bands are determined by their eigenvector orientations, which are perpendicular to each other, with G^- polarized along the strain axis as indicated in Figure 3d. The carbon−carbon bonds soften in the direction along the strain axis and thus become more sensitive to the applied loads. Further, the downshift rates of the G^- band in Figure 3b can reflect the local load-bearing status of the GO nanosheets during the tensile process more elaborately. For the as-received GO papers, the downshifted trend of the G^- band shows two-stage features: at low strains, they decrease linearly with a rate of ~4.2 cm^{-1} per 1% strain and once the strains exceed a certain point (~0.3%), the peak positions plateau until the final breakage of the samples. However, the shifted trend for the GA-treated papers decreases linearly through the whole strain region with a rate of ~14.6 cm^{-1} per 1% strain. By analyzing the Raman results in detail, we can further determine the load-bearing capabilities of the GO

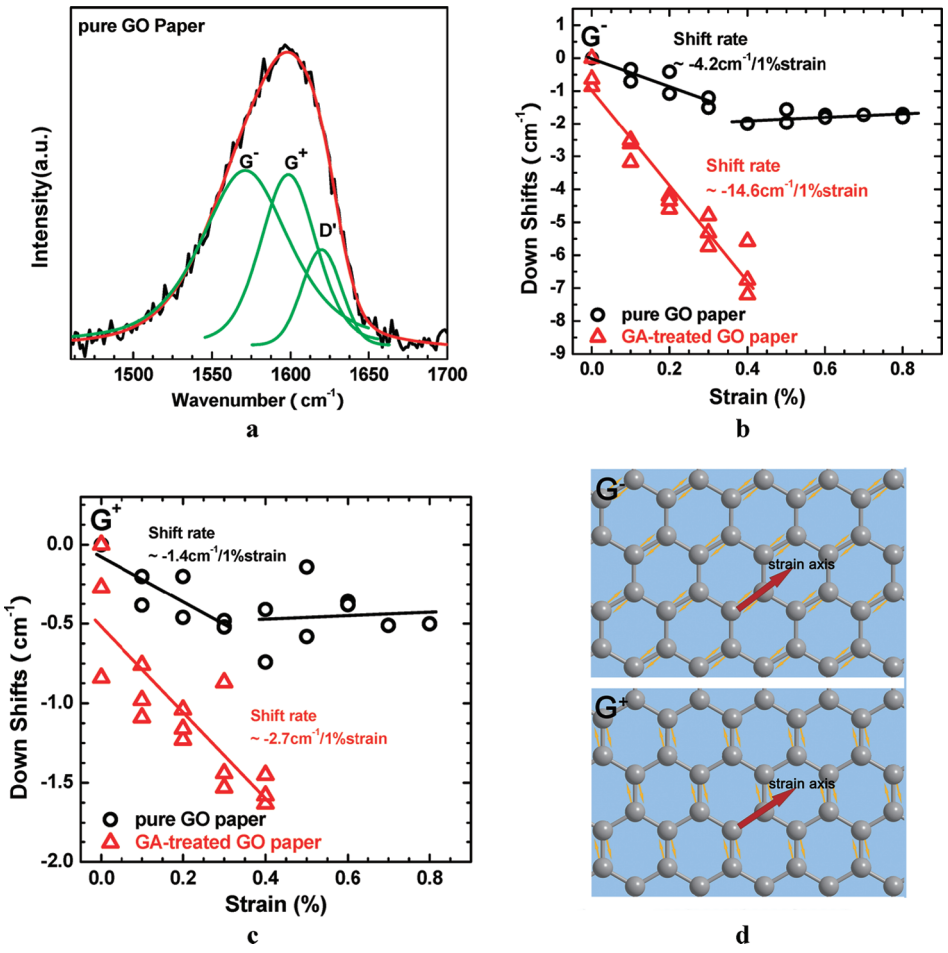

Figure 3. (a) Typical G band of the as-received GO paper fitted well with three peaks of G^-, G^+, and D′; the Raman shifts of G^- band (b) and G^+ band (c) as a function of applied strain; (d) eigenvectors of G^- and G^+ bands which are perpendicular to each other, with G^- polarized along the strain axis.[23]

nanosheets in the macroscopic papers from the following aspects. First, from the different shift rates of G^- band (at the low strain stage for the as-received GO paper), it can be inferred that the load-bearing capability of the GO nanosheets is visibly improved with the help of GA treatment. According to Mohiuddin's result, the average downshift rate of the G^- band for strained individual graphene is ~31.7 cm^{-1} per 1% strain,[23] which is higher than that of our as-received and GA-treated papers. The small downshift rates in our cases imply that the nanosheets' extensions only contribute partly to the macroscale strain of the GO paper. Here, we define the strain transfer factor (STF) as the ratio of downshift rate for macroscale papers to that for strained individual graphene sheets. The STF can give us a quantitative evaluation of how much macroscale strain comes from the extension of individual nanosheets. The STF for the as-received and the GA-treated paper is ~0.13 and ~0.46, respectively, which means the nanosheets in the latter bear ~3.5 times extensions of the ones in the former under the same strain level. The enhancement of interlayer adhesions after the GA molecules treatment could definitely improve the loading role of nanosheets in the macroscopic papers. Second, the final downshifts of the G^- band indicate the shear strength level of the neighboring nanosheets in the macroscale GO paper. In the case of as-received GO papers, the downshift of the G^- peak reaches ~1.5 cm^{-1} at a strain of ~0.3% and then plateaus even though more strain is applied. This transition implies that the applied loads have reached the averaged shear strength of the adjacent sheets, and further added stress will lead to the relative slippages rather than the extension of carbon−carbon bonds. However, the shifts for GA-treated papers decrease by ~7.0 cm^{-1} linearly until the final breakage. The larger final downshifts indicate the increased shear strength of adjacent nanosheets for GA-treated papers.

In fact, with the well-defined STF, we can further determine a numerical relationship between the moduli of the macroscale GO papers and the obtained downshift rates by a simple formula (derivation in Supporting Information):

$$E_{macro} = c\alpha\langle\cos^2\theta\rangle E_{nanosheet} \quad (1)$$

Where α is the STF, c is the volume fraction of the nanosheets in the macroscale papers, and $E_{nanosheet}$ is

TABLE 1. Comparisons of the Predicted Young's Modulus of As-Received and GA-Treated GO Papers from eq *1* with Experimental Results

			predicted modulus (GPa)			
specimens	volume fraction (*c*)	STF (*f*)	$\langle\cos^2\theta\rangle$ 0.5	$\langle\cos^2\theta\rangle$ 0.6−0.8	$\langle\cos^2\theta\rangle$ 0.9−1	experimental modulus (GPa)
as-received GO paper	∼0.3	0.13	7.8	9.4−12.5	14.0−15.6	9.1−13
GA-treated GO paper	∼0.23	0.46	21.2	25.4−33.8	38.1−42.3	26−34.7

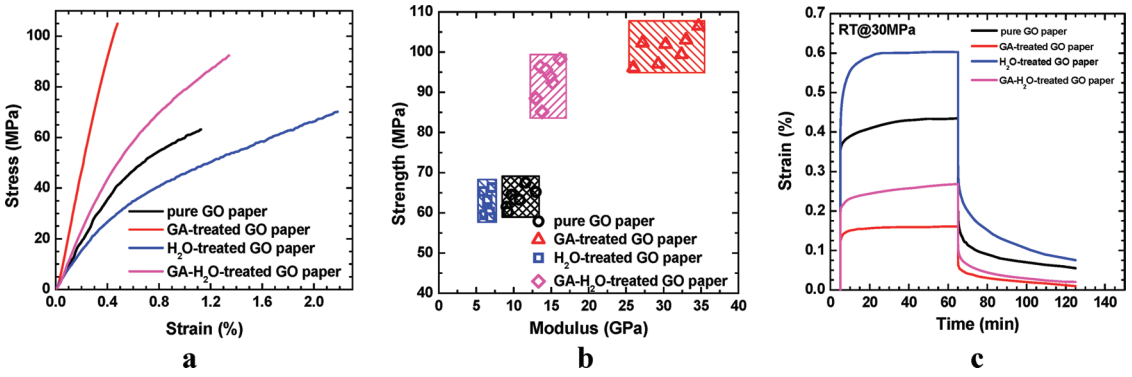

Figure 4. Mechanical properties of the as-received and modified GO papers: (a) typical stress−strain curves of tensile tests; (b) summary of moduli and strength for tested samples; (c) typical creep and recovery curves.

the average modulus of individual GO sheets; here we adopt 400 GPa.[28] The $\langle\cos^2\theta\rangle$ describes the orientation effect of nanosheets on the moduli of the macroscopic samples. In this predictive method, except STF, it also clarifies the influence of some other microstructure parameters, such as volume fraction (*c*) and orientation ($\langle\cos^2\theta\rangle$) of nanosheets, on the modulus of the macroscopic GO papers. Theoretically, the value of $\langle\cos^2\theta\rangle$ could be obtained by averaging the orientation angles of the nanosheets. At present, there is no experimental data to determine it strictly, so here we treat it as an unsettled parameter. In a 2D system, the complete random orientation gives $\langle\cos^2\theta\rangle$ a value of 0.5 and a uniform orientation of 1. Table 1 lists the predicted modulus given by eq 1 with different $\langle\cos^2\theta\rangle$ values. Compared with the experimental results, the predicted modulus fits the measured values very well with the $\langle\cos^2\theta\rangle$ value of 0.6−0.8, indicating the alignment of nanosheets within the macroscopic papers is mainly affected by the planar feature of nanosheets and the flow-directed filtration method itself.

Figure 4a presents the typical stress−strain curves of as-received and the modified GO papers. At least seven samples were tested for each specimen as summarized in Figure 4b. For example, the GA-treated GO paper has an average modulus of ∼30.4 GPa and a strength of ∼101 MPa. These values are, respectively, 190% and 60% higher than that of the as-received GO paper (modulus ≈ 10.5 GPa, strength ≈ 63.6 MPa). The enhancement both of stiffness and strength arise from the improved load-bearing capabilities of the GO nanosheets as a consequence of better interlayer adhesions. In addition, for the as-received GO paper, the ultimate tensile strain was ∼1.0% and the slope of the stress−strain curve obviously decreased beyond ∼0.3% strain level. Such behaviors reveal the onset of relative slippage between the neighboring nanosheets, which is consistent with the two-stage feature of G^- band shifted trend as shown in Figure 3b. By contrast, the stress−strain curve of the GA-treated GO paper behaved almost like a straight line with failure strain ≈ 0.4%, which was consistent with the G^- band-shifted trend presented in Figure 3b.

Recent studies have proven that the mechanical properties of GO papers strongly depend on its water content.[13,19,29,30] The interlamellar water molecules would reorient themselves in response to the external loads based on the hydrogen bonds, and this motion finally results in lower modulus of macroscale paper with higher water content.[19] In our opinion, the interlamellar water molecules could serve as efficient lubricants which weaken the interlayer adhesions and facilitate the slippages of nanosheets under external loading. As shown in Figure 4a, after treatment at relatively high humidity, the GO paper with higher water content has a lower tensile modulus of ∼6.5 GPa and an ultimate strain of ∼2.3%. Meanwhile, the strength is ∼62.3 MPa, almost the same as the as-received paper. Additionally, the larger failure strain infers the toughening role the interlamellar water molecules played, where a great deal of mechanical energy is dissipated during the frictional sliding of adjacent nanosheets. The calculated toughness of H_2O-treated GO papers is ∼1.0 MJ/m^3, which is twice as high as that of the as-received paper (∼0.5 MJ/m^3).

As narrated above, the improved loading roles of individual nanosheets with the help of GA molecules would effectively stiffen and strengthen the mechanical performance of the macroscopic GO papers. Contrarily, the interlamellar water molecules could weaken and

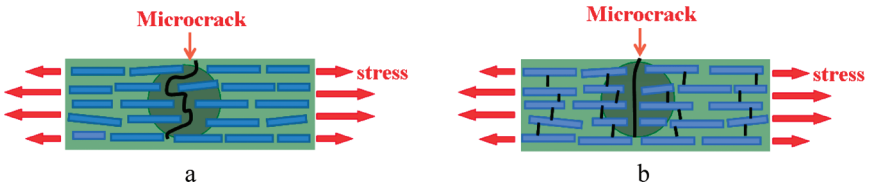

Figure 5. Schematic diagrams show fracture mechanisms for (a) as-received GO paper and (b) GA-treated GO paper.

toughen the paper through reorientation of the hydrogen bond. Herein, we try to combine these two effects together to tailor the mechanical behavior of GO papers. Namely, the paper is treated with a two-step method: (i) first, modify with the GA molecules and then (ii) entrap the water molecules by exposing the paper to a relatively high humidity of 98% for 3 days. As seen in the stress–strain curves in Figure 4a, the resulting GO paper is more flexible than the GA-treated paper and stiffer than the H_2O-treated paper. The obtained modulus and ultimate strength are ~14.4 GPa and ~93 MPa, respectively; besides, the elongation becomes ~1.3%. The toughness is calculated to be ~0.8 MJ/m^3, while that of the GA-modified paper is only ~0.3 MJ/m^3.

Moreover, the influence of interlayer adhesions on the load-bearing capabilities of nanosheets as well as the macroscopic mechanical behaviors of the GO papers could be identified through the conventional dynamic mechanical tests. Here the creep and recovery curves at 30 MPa in Figure 4c further reflect the relative slippages of adjacent layers of various GO paper specimens. Obviously, among the four different types of samples, the GA-treated GO paper exhibits the least residual deformation after recovery, which implies that the stronger interlayer adhesion could effectively restrain the slippage of neighboring nanosheets. However, for the H_2O-treated GO paper, both the creep strain and residual strain after recovery are much larger than that of the as-received GO paper. This result further demonstrates that the water molecules could stimulate the relative slippages of neighboring nanosheets. As expected, for GA-H_2O-treated GO paper, it exhibits larger creep strain than the GA-treated GO paper and smaller recovery strain than the H_2O-treated GO paper. Such variations in the interlayer adhesions would further impose influence on the fracture behaviors of the macroscopic GO papers.

Figure 5 illustrates the different microscopic structural fracture mechanisms for the strained GO papers with different interlayer adhesions. For example, the interlayer slippages would easily occur at the large applied strain level for the as-received and the H_2O-treated GO paper. So we have good reason to speculate that when strain is gradually applied to the specimen the wrinkled building sheets are stretched and extended to straight, then the adjacent sheets begin to slip relatively, and finally the microcrack emerges under the large applied strain and would enlarge through the interlayer spaces until the tensile failure (Figure 5a). During this process, the reorientation of interlamellar water molecules would activate the relative slippages and further dissipate the energy when microcracks emerge. Consequently, the H_2O-treated GO paper demonstrated larger failure strain and high toughness. As shown in Figure 5b, the situation of the GA-treated paper is different from the as-received GO paper as well as H_2O-treated GO paper, where almost no slippage would occur owing to the stronger interlayer adhesion. Once the microcracks emerged, the stress at the crack tip was concentrated, there was no way to dissipate the energy since the slippage of nanosheets was effectively constrained. The paper possessed a brittle feature, which was in accordance with the linearly shifted trend of Raman G^- band under tension. Therefore, the toughness of the GA-treated GO paper is the smallest among the various GO specimens.

In summary, the macroscopic GO papers were fabricated through a flow-directed filtration method. Small molecules, such as GA and water, were successfully introduced to the gallery regions and effectively tailored the interlayer adhesions of the GO papers. Both the tensile modulus and strength show significant improvements for the GA-treated GO papers, whereas decreased mechanical properties are observed for the H_2O-treated GO papers. After the combination of these two methods, a novel GO paper with strong and relative ductile properties was obtained. By applying *in situ* Raman spectroscopy to the strained macroscopic papers, we monitored the load-bearing capability of nanosheets before and after GA treatment, and further predicted the moduli of these macroscopic papers. Systematic mechanical tests confirmed that the enhancement of tensile moduli and strength of GA-treated GO paper arose from the improvement of interlayer adhesions. Moreover, on the basis of *in situ* Raman and mechanical results, the dependence of microscopic fracture mechanisms of the strained GO papers on the interlayer adhesions was inferred.

METHODS

GO was prepared from purified natural graphite (obtained from Qingdao Yingshida graphite Co., Ltd., with a particle size of 20 μm) by a modified Hummers method.[24] Under agitation, graphite powder (4 g) and sodium nitrate (3 g) were mixed with sulfuric acid (150 mL, 98 wt %) in an ice bath, and potassium permanganate (18 g) was slowly added to prevent the

temperature from exceeding 293 K. The reaction was kept at 293−303 K for 2 h with gas release, and then deionized water (300 mL) was gradually added. The resultant bright-yellow suspension was diluted and further treated with a H_2O_2 solution (500 mL, 3%), followed by centrifugation and careful washing to clean out remnant salt. Colloidal dispersions of individual GO sheets in water (3 mg/mL) were prepared with the aid of an ultrasonic cleaner.

Unmodified (as-received) GO paper was made by filtration of the resulting colloid (10 mL) through a cellulose membrane filter (47 mm in diameter, 0.22 μm pore size), followed by air drying and peeling from the filter. Samples of GO paper prepared in this manner were cut by a razor blade into strips (30 mm × 2 mm) and then dried at 60 °C for 12 h with a vacuum oven before further modifications or tests. Further treatment with GA was performed by exposure to GA vapors for 6−8 h at 37 °C. To study the hydration behavior of GO paper, the samples were placed in an environmental chamber (EYEL4, KCL 2000) at a relative humidity of 98% and 30 °C for 3 days. In addition, we employed the two-step method by first exposing GO paper to GA vapors and then keeping it at a higher humidity of 98% for 3 days.

Typical tapping-mode AFM measurements were performed using Dimension 3100. Samples for AFM images were prepared by depositing a dispersed GO/H_2O solution (2 μg/mL) onto a freshly cleaved mica surface and allowing it to dry in air. The cross section of GO paper specimen was studied by field-emission SEM (HITACHI S-4800). Spectral analysis of GO was characterized by FTIR spectroscopy (Spectrum One, PE, US) and XPS experiments (Mg Kα radiation, VG scientific ESCALab 220I-XL, UK). X-ray diffraction (XRD) measurements for paper samples were performed at room temperature using specular reflection mode (Cu Kα radiation, X'Pert PRO, PANalytical, Holland). A dynamic mechanical analyzer (TA, DMA Q800) was employed to evaluate the mechanical performances of GO paper. The static tensile tests were conducted in displacement ramp mode with a prestrain 0.01% and a ramp rate of 20 μm/min. Short time creep tests were performed in the tensile mode at room temperature with an applied stress of 30 MPa, and the creep strain was determined as a function of time (t_{creep} = 30 min, $t_{discovery}$ = 30 min).

Acknowledgment. The project was jointly supported by the National Key Basic Research Program of China (Grant No. 2007CB936803) and a key international collaboration project (Grant No. 2008DFA51220) of the Ministry of Science and Technology of China, key items of the Knowledge Innovation Project of the Chinese Academy of Sciences (Grant Nos. KJCX2-YW-M01 and KJCX2-YW-H21), and the National Natural Science Foundation of China (Grant Nos. 20874023, 51073044, and 9102301).

Supporting Information Available: Derivation of equation 1. This material is available free of charge *via* the Internet at http://pubs.acs.org.

REFERENCES AND NOTES

1. Patchkovskii, S.; Tse, J. S.; Yurchenko, S. N.; Zhechkov, L.; Heine, T.; Seifert, G. Graphene Nanostructures as Tunable Storage Media for Molecular Hydrogen. *Proc. Natl. Acad. Sci. U.S.A.* **2005,** *102*, 10439–10444.
2. Stankovich, S.; Dikin, D. A.; Dommett, G. H. B.; Kohlhaas, K. M.; Zimney, E. J.; Stach, E. A.; Piner, R. D.; Nguyen, S. T.; Ruoff, R. S. Graphene-Based Composite Materials. *Nature* **2006,** *442*, 282–286.
3. Lee, C.; Wei, X. D.; Kysar, J. W.; Hone, J. Measurement of the Elastic Properties and Intrinsic Strength of Monolayer Graphene. *Science* **2008,** *321*, 385–388.
4. Li, X. L.; Wang, X. R.; Zhang, L.; Lee, S. W.; Dai, H. J. Chemically Derived, Ultrasmooth Graphene Nanoribbon Semiconductors. *Science* **2008,** *319*, 1229–1232.
5. Stoller, M. D.; Park, S. J.; Zhu, Y. W.; An, J. H.; Ruoff, R. S. Graphene-Based Ultracapacitors. *Nano Lett.* **2008,** *8*, 3498–3502.
6. Novoselov, K. S.; Geim, A. K.; Morozov, S. V.; Jiang, D.; Zhang, Y.; Dubonos, S. V.; Grigorieva, I. V.; Firsov, A. A. Electric Field Effect in Atomically Thin Carbon Films. *Science* **2004,** *306*, 666–669.
7. Kim, K. S.; Zhao, Y.; Jang, H.; Lee, S. Y.; Kim, J. M.; Kim, K. S.; Ahn, J. H.; Kim, P.; Choi, J. Y.; Hong, B. H. Large-Scale Pattern Growth of Graphene Films for Stretchable Transparent Electrodes. *Nature* **2009,** *457*, 706–710.
8. Berger, C.; Song, Z. M.; Li, X. B.; Wu, X. S.; Brown, N.; Naud, C.; Mayou, D.; Li, T. B.; Hass, J.; Marchenkov, A. N.; *et al.* Electronic Confinement and Coherence in Patterned Epitaxial Graphene. *Science* **2006,** *312*, 1191–1196.
9. Stankovich, S.; Dikin, D. A.; Piner, R. D.; Kohlhaas, K. A.; Kleinhammes, A.; Jia, Y.; Wu, Y.; Nguyen, S. T.; Ruoff, R. S. Synthesis of Graphene-Based Nanosheets *via* Chemical Reduction of Exfoliated Graphite Oxide. *Carbon* **2007,** *45*, 1558–1565.
10. Compton, O. C.; Nguyen, S. T. Graphene Oxide, Highly Reduced Graphene Oxide, and Graphene: Versatile Building Blocks for Carbon-Based Materials. *Small* **2010,** *6*, 711–723.
11. Yang, Y. G.; Chen, C. M.; Wen, Y. F.; Yang, Q. H.; Wang, M. Z. Oxidized Graphene and Graphene Based Polymer Composites. *New Carbon Mater.* **2008,** *23*, 193–200.
12. He, H. Y.; Klinowski, J.; Forster, M.; Lerf, A. A New Structural Model for Graphite Oxide. *Chem. Phys. Lett.* **1998,** *287*, 53–56.
13. Dikin, D. A.; Stankovich, S.; Zimney, E. J.; Piner, R. D.; Dommett, G. H. B.; Evmenenko, G.; Nguyen, S. T.; Ruoff, R. S. Preparation and Characterization of Graphene Oxide Paper. *Nature* **2007,** *448*, 457–460.
14. Chen, C. M.; Yang, Q. H.; Yang, Y. G.; Lv, W.; Wen, Y. F.; Hou, P. X.; Wang, M. Z.; Cheng, H. M. Self-Assembled Free-Standing Graphite Oxide Membrane. *Adv. Mater.* **2009,** *21*, 3541–3541.
15. Chen, H.; Muller, M. B.; Gilmore, K. J.; Wallace, G. G.; Li, D. Mechanically Strong, Electrically Conductive, and Biocompatible Graphene Paper. *Adv. Mater.* **2008,** *20*, 3557–3561.
16. Zhu, Y. W.; Murali, S.; Cai, W. W.; Li, X. S.; Suk, J. W.; Potts, J. R.; Ruoff, R. S. Graphene and Graphene Oxide: Synthesis, Properties, and Applications. *Adv. Mater.* **2010,** *22*, 3906–3924.
17. Park, S.; Lee, K. S.; Bozoklu, G.; Cai, W.; Nguyen, S. T.; Ruoff, R. S. Graphene Oxide Papers Modified by Divalent Ions—Enhancing Mechanical Properties *via* Chemical Cross-Linking. *ACS Nano* **2008,** *2*, 572–578.
18. Park, S.; Dikin, D. A.; Nguyen, S. T.; Ruoff, R. S. Graphene Oxide Sheets Chemically Cross-Linked by Polyallylamine. *J. Phys. Chem. C* **2009,** *113*, 15801–15804.
19. Medhekar, N. V.; Ramasubramaniam, A.; Ruoff, R. S.; Shenoy, V. B. Hydrogen Bond Networks in Graphene Oxide Composite Paper: Structure and Mechanical Properties. *ACS Nano* **2010,** *4*, 2300–2306.
20. Ma, W. J.; Liu, L. Q.; Yang, R.; Zhang, T. H.; Zhang, Z.; Song, L.; Ren, Y.; Shen, J.; Niu, Z. Q.; Zhou, W. Y.; *et al.* Monitoring a Micromechanical Process in Macroscale Carbon Nanotube Films and Fibers. *Adv. Mater.* **2009,** *21*, 603–608.
21. Ma, W. J.; Liu, L. Q.; Zhang, Z.; Yang, R.; Liu, G.; Zhang, T. H.; An, X. F.; Yi, X. S.; Ren, Y.; Niu, Z. Q.; *et al.* High-Strength Composite Fibers: Realizing True Potential of Carbon Nanotubes in Polymer Matrix through Continuous Reticulate Architecture and Molecular Level Couplings. *Nano Lett.* **2009,** *9*, 2855–2861.
22. Tsoukleri, G.; Parthenios, J.; Papagelis, K.; Jalil, R.; Ferrari, A. C.; Geim, A. K.; Novoselov, K. S.; Galiotis, C. Subjecting a Graphene Monolayer to Tension and Compression. *Small* **2009,** *5*, 2397–2402.
23. Mohiuddin, T. M. G.; Lombardo, A.; Nair, R. R.; Bonetti, A.; Savini, G.; Jalil, R.; Bonini, N.; Basko, D. M.; Galiotis, C.; Marzari, N.; *et al.* Uniaxial Strain in Graphene by Raman Spectroscopy: G peak Splitting, Gruneisen Parameters, and Sample Orientation. *Phys. Rev. B* **2009,** *79*, 205433.
24. Xu, J.; Wang, K.; Zu, S.-Z.; Han, B.-H.; Wei, Z.-X. Hierarchical Nanocomposites of Polyaniline Nanowire Arrays on Graphene Oxide Sheets with Synergetic Effect for Energy Storage. *ACS Nano* **2010**, *4*, 5019.

25. Podsiadlo, P.; Kaushik, A. K.; Arruda, E. M.; Waas, A. M.; Shim, B. S.; Xu, J. D.; Nandivada, H.; Pumplin, B. G.; Lahann, J.; Ramamoorthy, A.; *et al.* Ultrastrong and Stiff Layered Polymer Nanocomposites. *Science* **2007,** *318*, 80–83.
26. Malard, L. M.; Pimenta, M. A.; Dresselhaus, G.; Dresselhaus, M. S. Raman Spectroscopy in Graphene. *Phys. Rep.-Rev. Sec. Phys. Lett.* **2009,** *473*, 51–87.
27. Kudin, K. N.; Ozbas, B.; Schniepp, H. C.; Prud'homme, R. K.; Aksay, I. A.; Car, R. Raman Spectra of Graphite Oxide and Functionalized Graphene Sheets. *Nano Lett.* **2008,** *8*, 36–41.
28. Gomez-Navarro, C.; Burghard, M.; Kern, K. Elastic Properties of Chemically Derived Single Graphene Sheets. *Nano Lett.* **2008,** *8*, 2045–2049.
29. Buchsteiner, A.; Lerf, A.; Pieper, J. Water Dynamics in Graphite Oxide Investigated with Neutron Scattering. *J. Phys. Chem. B* **2006,** *110*, 22328–22338.
30. Cerveny, S.; Barroso-Bujans, F.; Alegria, A.; Colmenero, J. Dynamics of Water Intercalated in Graphite Oxide. *J. Phys. Chem. C* **2010,** *114*, 2604–2612.